Silylene Defect at the Dihydrogen Terminated (100) Si Surface†

P. Belanzoni,*,‡ G. Giorgi,‡,§ A. Sgamellotti,‡ and G. F. Cerofolini‖

Department of Chemistry, University of Perugia, Via Elce di Sotto 8, 06123 Perugia PG, Italy, and CNISM and Department of Materials Science, University of Milano-Bicocca, Via Cozzi 53, 20125 Milano MI, Italy

Received: April 14, 2009; Revised Manuscript Received: August 27, 2009

Density functional calculations for both periodic slabs and different size cluster models of the hydrogen-terminated (100) surface of silicon are used to study a new configuration, formed by a silylene center interacting with vicinal silicon dihydrides through nonconventional hydrogen bonds. A comparison between slab-model and cluster-model approaches to modeling surface silylene defect formation processes is presented. The cluster models are used to analyze the structure and bonding of the silylene with a Lewis acid and base, showing the Zwitterionic nature of the defect. The silylene is also demonstrated to behave as a strong Brønsted acid. The stabilization of the silylene defect via interaction with species unavoidably present in the HF_{aq}-etching solution is investigated. Finally, the negative chemical shift observed by X-ray photoelectron spectroscopy in the HF_{aq}-etched (100) Si surface is attributed to the occurrence of silylene defect.

1. Introduction

Integrated circuits are almost exclusively constructed on (100)-oriented single-crystalline silicon substrates. This explains by itself why the (100) silicon surfaces have been subjected to intense experimental and theoretical studies. Moreover, such surfaces (and especially the hydrogen-terminated ones) have great fundamental interest for the various phases therein observed.

Procedures for the preparation of chemically homogeneous, atomically flat, nearly ideal, hydrogen terminated, (100) Si surfaces are known. The route commonly employed in the laboratory practice requires the demolition of the native oxide by heat treatments at high temperature ($T > 1000$ °C), and the subsequent exposure of the resulting (terraced and reconstructed) 2×1 (100) Si_2 surface to atomic hydrogen. According to the temperature of the surface, the exposure to a few langmuirs of atomic hydrogen H results in the following configurations:[1]

- 1×1 (100) SiH_2, with full dihydride coverage, at 300 K;
- 3×1 (100) SiH_2 $(SiH)_2$, with a sequence of dihydride-monohydride-dimer pairs, at 400 K; or
- 2×1 (100) $(SiH)_2$, with a full mohydride-dimer coverage, at 600 K.

In a narrow temperature interval (between 420 and 530 K) the exposure of rough surfaces to atomic hydrogen results in a form of buried hydrogen.[2]

As far as the use of atomic hydrogen is impractical, alternative processes based on the substitution of H_2 for H have been described. According to the experimental conditions, the exposure of the silicon surface to *molecular hydrogen* at subatmospheric pressure has been reported to result in 2×1 (100) $(SiH)_2$[3] or 1×1 (100) SiH_2 surfaces.[4]

None of the above processes has, however, found technological applications. Rather, the oldest process (the etching of the native oxide with aqueous solution of HF, HF_{aq}) has remained unrivalled in practice. As shown by the extended analysis based on infrared (IR) spectroscopy, the HF_{aq} etching results in prevailing SiH_2 terminations but contains also SiH [on (111) facets produced by the attack] and SiH_3 terminations, and siloxo defects.[5]

TABLE 1: Chemical Shift $\Delta\xi$ and Line Width w of All Considered Features for the HF_{aq}-Etched Surface

energy	$Si^{-\prime}$	Si^{0}	$Si^{\prime}$	$Si^{2\prime}$	$Si^{3\prime}$	Si^{1}	Si^{2}	Si^{3}	Si^{4}
$\Delta\xi$ (eV)	−0.27	0.00	0.13	0.28	0.47	1.01	1.84	2.86	3.63
w (eV)	0.42	0.35	0.26	0.28	0.29	0.72	0.65	0.72	1.03

TABLE 2: XPS Features Observed at the HF_{aq}-Etched (100) Si Surface and the Chemical Configurations Assigned to Them

$Si^{\prime}$	$Si^{2\prime}$	$Si^{3\prime}$	Si^{1}	Si^{2}	Si^{3}	Si^{4}
SiH	Si(H)OH	SiH_2	SiH_3 + Si(OSi)	$Si(OSi)_2$	$Si(OSi)_3$	$Si(OSi)_4$

The wide heterogeneity of the HF_{aq}-etched (100) Si surface, manifested by IR spectroscopy, is also confirmed by X-ray photoelectron spectroscopy (XPS). An angle-resolved XPS analysis of device-quality (100) Si substrates gave indeed evidence for eight superficial lines (in addition to that of elemental silicon Si^0), hereinafter referred to as follows: $Si^{-\prime}$, $Si^{k\prime}$ (with $k = 1, 2, 3$), and Si^n (with $n = 1, ..., 4$); to avoid confusion, the symbols used here are not the same as in the original papers. Table 1 lists the corresponding chemical shifts $\Delta\xi$ of 2p core electrons (with respect to the binding energy of elemental silicon) and line widths w[6].

As discussed in Appendix A, while all features with positive chemical shift can be attributed, on the basis of ab initio calculations of net charge and Madelung potential, to species whose presence was asserted by infrared spectroscopy too (see Table 2), $Si^{-\prime}$ (the unique feature with negative chemical shift) cannot be assigned to any reported species.[7]

Remarkably enough, feature $Si^{-\prime}$ has been observed not only on HF_{aq}-etched silicon[6] but also on silicon treated in H_2 at subatmospheric pressure (around 10^4 Pa) at high temperature (850−1100 °C).[4,8,9]

In a previous work by us,[10] we proposed that the occurrence of silylene centers with a partial negative charge could be

† Part of the "Vincenzo Aquilanti Festschrift".

* To whom correspondence should be addressed. Electronic address: paola@thch.unipg.it.

‡ University of Perugia.

§ Current address: Department of Chemical System Engineering, Graduate School of Engineering, The University of Tokyo, Tokyo 113-8656, Japan.

‖ University of Milano-Bicocca.

10.1021/jp903433e
Published on Web 09/28/2009

considered as being responsible for the XPS feature with negative chemical shift observed at the hydrogen-terminated (100) Si surface. This work represents an extension of these earlier studies on the silylene defect[10] in that an extensive comparison of cluster and slab models is made for the silylene defect formation processes, to monitor the convergence of the energies involved with increasing slab and cluster size, and the convergence of the chemical features, such as acidic or basic strength and XPS chemical shift, of the silylene defect with increasing cluster size.

This work is addressed to assess the adequacy of the considered cluster model to study a range of topics related to the silylene defect, including structures, electronic states and chemical features, and to verify whether or not $Si^{-\prime}$ can be attributed to some form of silylene silicon. The assignation of $Si^{-\prime}$ to this species stands on the proposal by Cerofolini and Meda that the HF_{aq} etching of the native oxide of the (100) Si surface leaves, in addition to the silanic and siloxo terminations, silylene centers where silicon is covalently bonded to its two underlying silicon atoms only.[11]

To verify whether or not cluster models may be used to study the chemical features of silylene centers that can indeed occur on the 1×1 (100) SiH_2 surface,[10] we have performed a set of calculations in the framework of density functional theory (DFT): in a class of calculations (essentially devoted to establish the thermodynamic stability of the various configurations considered) the surface was modeled with a two-dimensional slab of atoms with periodic boundary conditions (PBC); in another class of calculations (essentially devoted to investigate the chemical features of the silylene defect) the local configurations were modeled with siladamantane clusters of different sizes. The cluster models allow us to use the Voronoi deformation density (VDD) method as implemented in the ADF package to calculate the atomic charge,[12] a fundamental quantity for XPS features, thus permitting a realistic evaluation that would not be feasible with the slab models using SIESTA code, where only the Mulliken population analysis is available. Due to the strong dependency of calculated charges on the assumed basis set, the Mulliken population analysis is indeed useless for a quantitative rationalization of the XPS chemical shift data.

2. Calculations

State-of-the-art calculations were performed in the frame of density functional theory (DFT) modeling the various surface configurations using slabs or clusters.

2.1. Slab Models. For our slab-model calculations we used the SIESTA code[13−15] and the Perdew−Burke−Ernzerhof (PBE) exchange−correlation functional.[16] Four slab models containing, respectively, 96, 168, 192, and 384 Si atoms per supercell, were employed. Use of such a large supercell is important for establishing convergence with respect to supercell size. Each supercell contained 8, 14, until 16 layers of Si atoms, each formed by 12 (24 for one 16 layers slab model) Si atoms (cell size: 11.5×15.4 Å^2); the first layer was terminated with the amount of hydrogen atoms required to attain the wanted termination and reconstruction. The last layer was terminated with the hydrogen atoms required to saturate silicon dangling bonds with no stress; the unsaturation of lateral bonds was taken into account imposing two-dimensional periodic conditions. A vacuum layer of 12 Å has been added in all our slab models. Norm-conserving pseudopotentials[17] were employed to replace core electrons; double-ζ basis set plus polarization has been used for valence electrons. Both pseudopotentials and basis sets have been tested in previous papers.[18,19] A mesh cutoff of 200 Ry has been used in conjunction with 0.04 eV/Å force convergence threshold in the ion and unit cell relaxation. All the atoms of the slabs have been fully optimized with a conjugate gradient minimization with a $2 \times 2 \times 1$ Monkhorst−Pack k-points sampling scheme.[20]

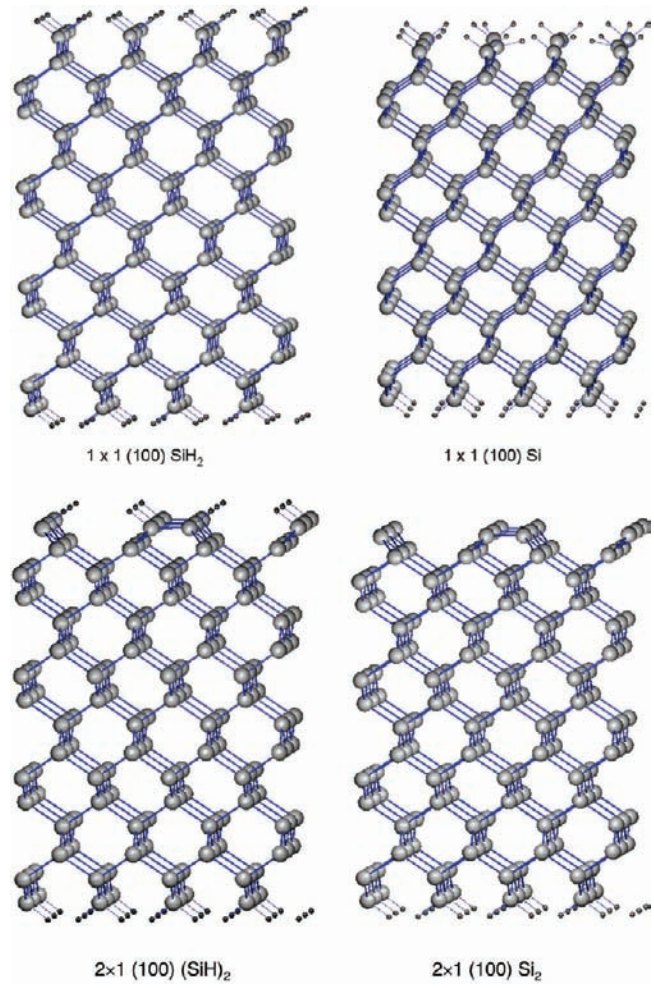

Figure 1. Structures of the considered Si (100) surfaces.

TABLE 3: Binding Energy per H_2 Molecule Associated with Hydrogen Desorption for Different Size Slab Models

slab size	ΔE_1(12/12) (eV)	ΔE_2(12/12) (eV)	ΔE_3(2/12) (eV)
8 × 12	−0.09	+1.88	
14 × 12	−0.16	+2.32	+0.84
16 × 12	−0.17	+2.32	+0.83
16 × 24			+0.86
	ΔE_1(2/12) (eV)	ΔE_2(2/12) (eV)	ΔE_3(2/12) (eV)
16 ×12	−0.49	+1.80	+0.83

2.2. Cluster Models. Three different size cluster models of hydrogen-terminated silicon atoms forming fused cyclohexasilanes[21] have been considered in the present study. The smallest cluster, Si_9H_{14}, has a single surface dimer, the intermediate sized $Si_{16}H_{22}$ cluster model has three surface Si atoms along a single row, and the largest $Si_{58}H_{62}$ cluster model has three rows of three Si atoms in the surface. For each cluster model, four different geometrical structures were considered, corresponding to different configurations: the dihydride SiH_2 1×1 (100); the monohydride $(SiH)_2$ 2×1 (100); the silylene Si 1×1 (100) defect; and the clean Si_2 2×1 (100) configuration. DFT calculations with the Becke−Perdew (BP86) exchange−correlation functional[22−24] were performed using the Amsterdam density

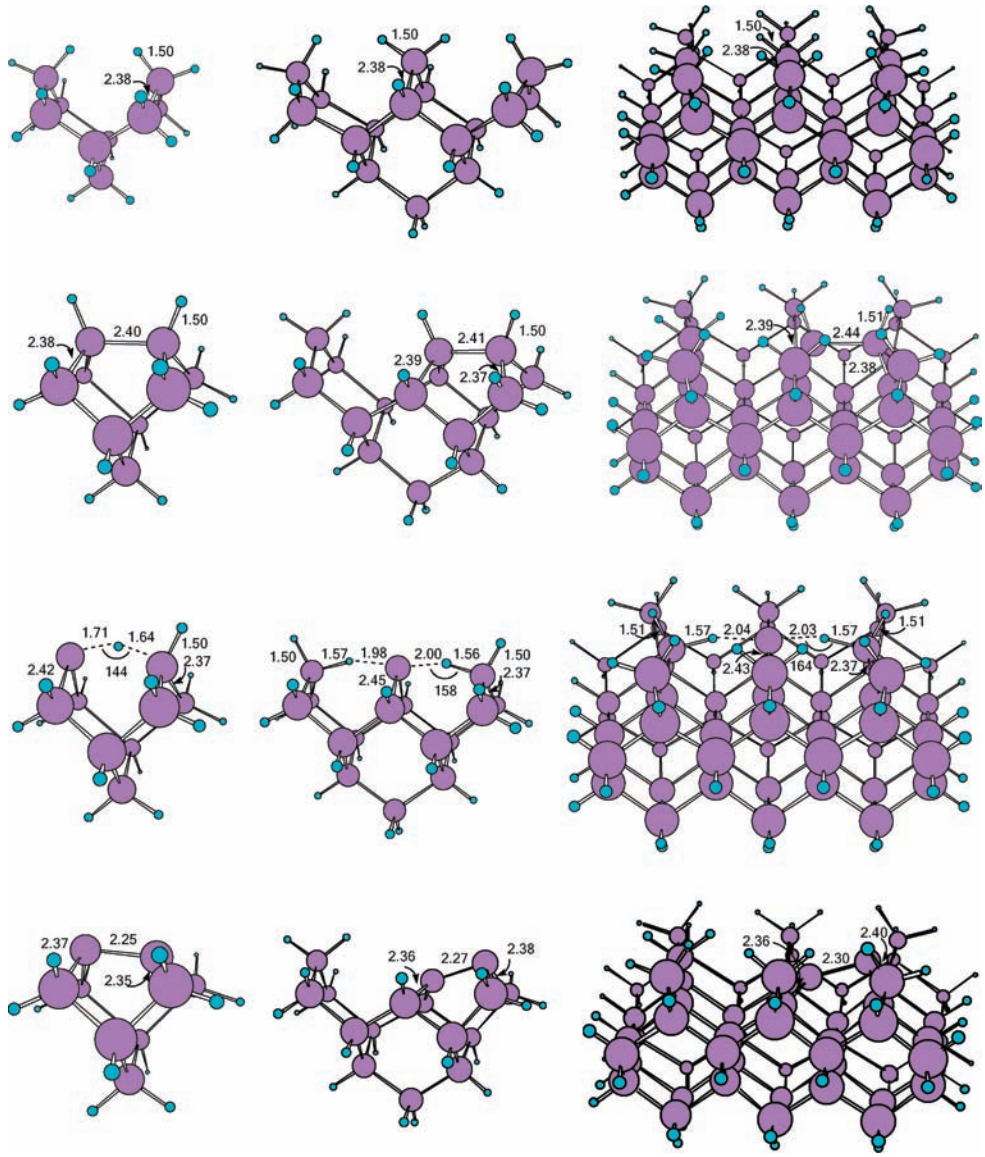

Figure 2. Structures and relevant geometrical parameters (Å) in the considered siladamantane cluster models of different sizes in different superficial configurations: dihydride (top), monohydride and silylene defect (middle), clean (bottom).

functional (ADF) program package 2007.1.[25−29] In the calculations, the molecular orbitals were expanded in a Slater-type STO basis set of triple-ζ doubly polarized TZ2P quality for all atoms. The core orbitals were kept frozen up to 2p for Si, or 1s for O, B, F, and N. Convergence criteria for full geometry optimizations were 1×10^{-3} hartrees in the total energy, 5×10^{-4} hartrees $Å^{-1}$ in the gradients, 1×10^{-2} Å in bond lengths, and 0.20° in bond angles. In all cases no symmetry was imposed and the stability of the structures was checked by performing a normal-mode analysis and checking that all vibration frequencies are positive for the Si_9H_{14} and $Si_{16}H_{22}$ cluster models; the $Si_{58}H_{62}$ cluster models were too large for feasible frequency calculations. The calculated equilibrium structures for all the Si_9H_{14} and $Si_{16}H_{22}$ cluster models are true minima, except when explicitly otherwise specified. For stability issues, the internal energy E_{int} was calculated correcting the electronic energy E with the vibrational ($E^0_{vib} + E_{vib}$), rotational (E_{rot}), and translational (E_{trans}) contributions,

$$E_{int} = E^0_{vib} + E_{vib} + E_{rot} + E_{trans}$$

After that, the enthalpy H and Gibbs free energy G per molecule were calculated from standard thermodynamic relationships, $H = E_{int} + k_BT$ and $G = H - TS$ where k_B is the Boltzmann constant and S is the entropy. In many instances, however, we observe that reactants and products differ from one another by low energies ΔE. Since we often consider adsorption processes from gas phases, where we may reasonably estimate a change of entropy related to the loss of translational degrees of freedom, we have to ignore the related change of Gibbs free energy ΔG^0, and the most convenient comparison is that between ΔE and ΔH^0.

The ground state spin configuration of all clusters, including the silylene defect, is a singlet. However, for the silylene defect, a triplet spin state has been calculated that is above the singlet ground state for the three models by 0.8−0.9 eV and corresponds to a geometry structure where the two hydrogen atoms are strongly symmetric; i.e., both hydrogen atoms are in the usual silanic configuration, with the two unpaired electrons localized on the silylene Si.

The Voronoi deformation density (VDD) method, as implemented in the ADF package, was chosen for computing atomic

TABLE 4: Partial Charge (VDD) Distribution on Superficial Silicon and Hydrogen Atoms in the Site Subject to Hydrogen Desorption for Different Size Cluster Models

cluster size	Si_{sil}	H_{bridge}	Si	H
		Dihydride		
Si_9H_{14}			0.11	−0.05
$Si_{16}H_{22}$			0.12	−0.03
$Si_{58}H_{62}$			0.12	−0.03
		Monohydride		
Si_9H_{14}			0.03	−0.04
$Si_{16}H_{22}$			0.06/0.03	−0.05
$Si_{58}H_{62}$			0.05/0.04	−0.05
		Silylene Defect		
Si_9H_{14}	−0.05	0.04	0.11	−0.05
$Si_{16}H_{22}$	−0.06	0.03/0.04	0.09	−0.05
$Si_{58}H_{62}$	−0.08	0.03	0.11	−0.04
		Clean		
Si_9H_{14}			−0.11(up)	−0.01(down)
$Si_{16}H_{22}$			−0.13(up)	0.05(down)
$Si_{58}H_{62}$			−0.14(up)	0.07(down)

charges in the clusters, thus avoiding the unwanted dependence on the basis set suffered by Mulliken population analysis.[12]

3. Slab vs Cluster Model Results

Figure 1 provides information on the structures of the surfaces as result from the slab model calculations.

The stability of the results with respect to the size of the slab was checked by comparing the stabilities of 1 × 1 (100) SiH_2 and 2 × 1 (100) $(SiH)_2$ toward loss of H_2 for slabs with 8, 14, or 16 layers, as shown in Table 3. The stability is determined by the change of total binding energies for the following reactions

$$\underset{1\times1\ (100)}{2SiH_2} \xrightarrow{\Delta E_1(12/12)} \underset{2\times1\ (100)}{(SiH)_2} + H_2 \qquad (1)$$

$$\underset{2\times1\ (100)}{(SiH)_2} \xrightarrow{\Delta E_2(12/12)} \underset{2\times1\ (100)}{Si_2} + H_2 \qquad (2)$$

with $2m/n$ denoting the loss of $2m$ hydrogen atoms (as m H_2 molecules) from a superficial lattice of n silicon atoms.

TABLE 6: HOMO and LUMO Energies and Percentage Composition for the Three Different Size Clusters in Terms of Silylene Si_{sil}, Vicinal Silane Si_{silane}, Si Atoms Bond to Silylene Si $_{bond}$, and Si on Layers below the Surface Si_{layers}[a]

	E (eV)	Si_{sil}	Si_{silane}	Si_{bond}	Si_{layers}
		Si_9H_{14}			
HOMO	−5.195	54	4	12	8
LUMO	−3.087	48	31		
		$Si_{16}H_{22}$			
HOMO	−5.075	51	4	10	
LUMO	−3.072	40	28		
		$Si_{58}H_{62}$			
HOMO	−4.882	44	2	13	14
LUMO	−3.150	39	22	4	10

[a] Only the main contributions are reported.

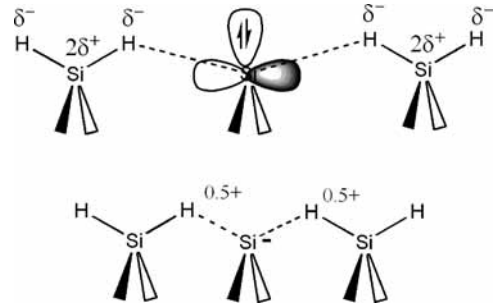

Figure 3. Silylene defect at the 1 × 1 (100) SiH_2 surface: structural formula (top) and Lewis resonance formula (bottom).

The calculations provided stable results when the slab was thicker than 14 atoms. The convergence with slab layers is less than or equal to 0.01 eV. Having gained confidence in the adequacy of our slab model 16 × 12 in the description of the hydrogen-terminated (100) surface of silicon, we can use it for the description of the defects thereon. To compare our slab model results with the cluster model results, we need to compute the corresponding ΔE_1 and ΔE_2 with $2m = 2$, i.e., the formation energy of the isolated monohydride dimer and of the isolated clean dimer, for the 16 × 12 slab model. The formation of the isolated monohydride dimer is thermodynamically favored with respect to the formation of the homogeneous phase:

TABLE 5: Binding Energy ΔE (in Gas Phase, 0 K, 0 atm), Enthalpy ΔH^0 (298 K, 1 atm), and Gibbs Free Energy ΔG^0 (298 K, 1 atm) per H_2 Molecule Associated with Hydrogen Desorption for Different Size Cluster Models

cluster size	$2/n$	$\Delta E_1(2/n)$ (eV)	$\Delta E_2(2/n)$ (eV)	$\Delta E_3(2/n)$ (eV)	$\Delta E_4(2/n)$ (eV)
Si_9H_{14}	2/2	+0.20	+2.00	+1.67	−1.47
$Si_{16}H_{22}$	2/3	+0.15	+1.96	+1.54	−1.39
$Si_{58}H_{62}$	2/9	+0.18	+2.00	+1.50	−1.30
cluster size	$2/n$	$\Delta H_1^0(2/n)$ (eV)	$\Delta H_2^0(2/n)$ (eV)	$\Delta H_3^0(2/n)$ (eV)	$\Delta H_4^0(2/n)$ (eV)
Si_9H_{14}	2/2	−0.03	+1.77	+1.35	−1.39
$Si_{16}H_{22}$	2/3	−0.12	+1.77	+1.19	−1.31
cluster size	$2/n$	$\Delta G_1^0(2/n)$ (eV)	$\Delta G_2^0(2/n)$ (eV)	$\Delta G_3^0(2/n)$ (eV)	$\Delta G_4^0(2/n)$ (eV)
Si_9H_{14}	2/2	−0.31	+1.36	+1.04	−1.35
$Si_{16}H_{22}$	2/3	−0.34	+1.29	+0.90	−1.24
			Slab		
16 × 12	2/12	−0.49	+1.80	+0.83	−1.32
			Cluster (Slab)[a]		
Si_9H_{14}	2/2			+1.81	
$Si_{16}H_{22}$	2/3			+1.59	
$Si_{58}H_{62}$	2/9			+1.52	

[a] These data refer to cluster model calculations at exactly the same level of theory as the slab model calculations.

$$\underset{1\times1\ (100)}{2SiH_2} \xrightarrow{\Delta E_1(2/12)} \underset{2\times1\ (100)\ \text{defect}}{(SiH)_2} + H_2{:}\Delta E_1(2/12) = -0.49\ \text{eV} \quad (3)$$

The binding energy difference $\Delta E_2(2/12)$ involved in the desorption of H_2 from an *isolated* superficial monohydride dimer at the 2×1 (100) surface is

$$\underset{2\times1\ (100)}{(SiH)_2} \xrightarrow{\Delta E_2(2/12)} \underset{2\times1\ (100)}{Si_2} + H_2{:}\Delta E_2(2/12) = +1.80\ \text{eV} \quad (4)$$

Focusing now our attention on the silylene defect, in which limit such defects may be considered really isolated is specified by the periodic conditions: for the monohydride dimer we are considering a situation where 2/12 of the superficial atoms occur in dimers, whereas for the silylene we are actually simulating a situation where 1/12 of the surface is covered by such defects. For the slab generated by the 16×12 slab model the binding energy difference $\Delta E_3(2/12)$ involved in the desorption of 2 hydrogen atoms (as H_2 molecule) from a *single* superficial silicon dihydride atom at the 1×1 (100) surface is given by

$$\underset{1\times1\ (100)}{SiH_2} \xrightarrow{\Delta E_3(2/12)} \underset{1\times1\ (100)\ \text{defect}}{Si} + H_2{:}\Delta E_3(2/12) = +0.83\ \text{eV} \quad (5)$$

Doubling the number of Si atoms on each layer, namely on going from a 16×12 to a 16×24 slab model, gives the convergence in energy for $\Delta E_3(2/12)$ as 0.03 eV (see Table 3). We should note that, due to computer resource limits, stopping at a 16×12 supercell can be considered reasonable convergence.

In an attempt to single out the width of the defect band, we found that the defect is not localized but rather dispersed, due to interaction of the defect with down layer Si atoms.

Thus although the calculations have provided evidence for silylene as an energetically possible defect of the 1×1 (100)SiH_2 surface, they do not give any information on the activation energy of this process; however, denoting with E_b^{Si-H} and E_b^{H-H} the Si−H and H−H bond-dissociation energies ($E_b^{Si-H} \simeq 3.6$ eV and $E_b^{H-H} = 4.4$ eV), if relaxation of nearby species occurs after H_2 desorption, the energy barrier to be overcome for silylene formation is about $2E_b^{Si-H} - E_b^{H-H} \simeq 2.8$ eV. The silylene defect is thus expected to form *under thermal activation* on the laboratory time scale (e.g., 10^3 s) only at high temperature (10^3 K). Since in a vacuum all hydrogen terminations are totally destroyed at these temperatures, silylene defects may form only at high H_2 pressures (as in the experiments of refs 4, 8, and 9). At room temperature the formation of this species is possible only along highly energetic reaction pathways, the etching with HF_{aq}[11] or photodesorption.

As follows from (1) and (2), the decay of this defect to a 2×1 (100) $(SiH)_2$ dimer by reaction with a nearby silicon dihydride is thermodynamically allowed, the energy excess $-\Delta E_4(12/12)$ of the silylene with respect to the monohydride dimer being of +1.43 eV. The formation of the monohydride dimer from an isolated silylene defect for the 16×12 slab model is also thermodynamically favored:

$$\underset{1\times1\ (100)\text{silylene}}{Si + SiH_2} \xrightarrow{\Delta E_4(2/12)} \underset{2\times1\ (100)\ \text{defect}}{(SiH)_2} \quad \Delta E_4(2/12) = -1.32\ \text{eV} \quad (6)$$

Of course, this datum concerns only the thermodynamic stability of the silylene defect at the 1×1 (100) SiH_2 surface. It is, however, noted that reverting the 1×1 (100) surface to the 2×1 (100) requires in general a strong thermal activation, so that metastable silylene defect could actually occur. The actual stability of the silylene defect will be considered later.

Stick-and-ball views of optimized cluster structures are shown in Figure 2. The three different size cluster models, in the four different geometrical structures mimicking the considered superficial configurations, are depicted; main geometrical parameters are also shown. VDD atomic charges on superficial silicon and hydrogen atoms in the site subject to H_2 abstraction are reported in Table 4 for all different size clusters. The calculated charges are found to slightly change while increasing the cluster size. Table 5 summarizes the formation energy $\Delta E_i(2/n)$ ($i = 1-4$) (0 K, 0 atm) of reactions 3−6, and the corresponding ΔH^0 and ΔG^0 (at 298 K, 1 atm) as a function of cluster size which are compared to the ΔE_i ($i = 1-4$) calculated for the 16×12 slab model with $2m = 2$. It should be pointed out that for a reasonable comparison the clusters are used as models for the isolated defects.

As shown in Table 5, while the data of formation energy ΔE_2 and ΔE_4 for the cluster models are in close agreement with the values calculated for the slab, the ΔE_1 and ΔE_3 are far from converging to the slab values. It is, however, worthwhile to note that the disagreement is drastically reduced if the formation enthalpy values ΔH_i^0 are used to evaluate the stability of the clusters. For the maximum cluster size, $Si_{58}H_{62}$, ΔH_i^0 and ΔG_i^0 could not be calculated due to the heavy computational effort required for frequency calculations. Given the different ingredients (basis sets, exchange-correlation functionals, etc.) involved in the two sets of calculations, slab and cluster model approaches, the agreement in the general trend can be considered highly satisfactory. A case where the slab and cluster models could be directly compared can be useful to this analysis. A single point calculation has been performed on Si_9H_{14}, $Si_{16}H_{22}$, and $Si_{58}H_{62}$ optmized geometries, on both dihydride and silylene defect configurations, to compute $\Delta E_3(2/n)$ using the SIESTA program; i.e., we did cluster model calculations at exactly the same level of theory as the slab model calculations. The results are $\Delta E_3 = 1.81$ eV for Si_9H_{14}, $\Delta E_3 = 1.59$ eV for $Si_{16}H_{22}$, and $\Delta E_3 = 1.52$ eV for $Si_{58}H_{62}$. These values are very close to 1.67, 1.54, and 1.50 eV (see $\Delta E_3(2/n)$ in Table 5) calculated, respectively, for Si_9H_{14}, $Si_{16}H_{22}$, and $Si_{58}H_{62}$ using ADF code.

A trend toward a smaller formation energy of the silylene defect is recognized with increasing the size of the cluster models. An MO analysis of the HOMO and LUMO of the three different size clusters containing the silylene defect is shown in Table 6. Although both the HOMO and LUMO are mainly localized on silylene, a general trend toward a delocalization of the defect can be observed as the cluster size increases. This behavior is particularly evident for the $Si_{58}H_{62}$ cluster whose HOMO and LUMO delocalize on the silicon atoms belonging to the layers below the surface. The delocalization of the LUMO over Si atoms of the cluster is in agreement with the fact that the negative charge on silylene Si due to interaction with hydroxyl anion (see section 5) rapidly decreases as the cluster size increases, thus indicating a delocalization of the negative charge over the cluster.

We can conclude that the considered clusters may be safely used as models for analyzing chemical features of the isolated defects.

Moreover, other quantities, like internuclear distances (see Figure 2) and net charges (see Table 4), were found to slightly change while increasing the cluster size. Since we are mainly interested in net charges and Madelung potentials, it is thus reasonable to take data resulting from the smallest Si_9H_{14} cluster modeling for assigning XPS features (see Appendix A).

4. Silylene Chemistry

Both the slab and cluster pictures of the silylene defect show that the hydrogen atoms in both nearby silicon dihydrides are notably asymmetric: whereas in each silicon dihydride one hydrogen is in the usual silanic configuration, the other is at a bond distance of silylene silicon too (see Figure 3, top). The configuration of each hydrogen coordinated to silylene silicon is in a configuration reminiscent of that in electron-deficient compounds like diborane; alternatively, the hydrogen may be viewed as an off-axis bond-centered proton in a strongly relaxed Si−Si bond.

4.1. Nature of the Hydrogen Bridge. The fact that hydrogen with positive partial charge form hydrogen bonds is too well-known to need a discussion. The fact that hydrogen with negative partial charge may form nonconventional hydrogen bonds is less known, but nonetheless well established.[30] The fact that the hydrogen involved in a highly covalent silanic bond may form a nonconventional hydrogen bond is even less trivial. The Lewis acidity of silylene is so strong as to attract the silanic hydrogen in its vicinity and to form nonconventional hydrogen bond. An exact Lewis resonance formula can be assigned to the silylene defect at the 1 × 1 (100) SiH_2 surface depicted at the bottom of Figure 3.

This structure is understood by observing that whereas the silicon dihydrides are in their usual electronic configuration, the divalent silylene silicon, which prefers to exist as a singlet, with the lone pair of the electrons as the HOMO and an empty p orbital as the LUMO, may complete its outer shell only via the acceptance of negative charge from neighboring silanic hydrogens. Even though donation by silanic hydrogen may seem strange, it is understood in terms of the Lewis acidity of the silylene center. In fact, since silylene misses an electron pair, to fill its outer electron shell silicon accepts the donation of an electron pair from any base to form Lewis acid−base complexes.

4.2. Zwitterionic Nature of Silylene. The amphoteric nature of silylene is well-known since the investigation of Raghavachari and co-workers.[31,32] In the following it is investigated "titrating" the silylene with Lewis base and acid.

4.2.1. Silylene as a Lewis base. To probe the base strength of the silylene defect at the 1 × 1 (100) SiH_2 surface, we used BF_3 because it is a strong Lewis acid and is sufficiently small as not to suffer from steric constraints. The silylene base was titrated in terms of the bond-formation energy of the resulting adduct. For the three clusters $Si_9H_{14}BF_3$, $Si_{16}H_{22}BF_3$, and $Si_{58}H_{62}BF_3$ the calculations provided the structures shown in Figure 4 (right), where VDD charges on silylene (Si_{sil}) and silanic silicon (Si) and hydrogen (H_{bridge}) are also reported, and gave a bonding energy ΔE of −0.13 eV for the smallest, −0.14 eV for the intermediate and −0.15 eV for the larger cluster, as shown in Table 7. The corresponding formation enthalpy ΔH^0 have been calculated for $Si_9H_{14}BF_3$ and $Si_{16}H_{22}BF_3$ and are very close to the ΔE values, showing a slightly exothermic process, whereas the corresponding ΔG^0 are positive, which would indicate a non spontaneous process. As noted in section 2.2, in our gas phase approximation we consider the ΔH^0, namely the electronic effects, to be more significative than ΔG^0.

It should also be noted that frequency calculation on $Si_{16}H_{22}BF_3$ gives two small negative values; thus the structure is not a true minimum.

Evidence of the involvement of the lone electron pair of silylene silicon in bonding to boron is immediately understood from the planar trigonal coordination around the silylene silicon. Silylene acts as a Lewis base through donation of the lone electron pair to boron, thus enhancing the attraction of silanic hydrogen atoms. Evidence is given by the facts that the distance between silylene silicon and silanic hydrogen slightly decreases with respect to bare silylene and the VDD charge on silylene silicon is close to zero with H_{bridge} bearing more positive charge in the three cluster models. However, the two calculated ΔH^0 values indicate that the silylene−BF_3 adducts are slightly stable, thus pointing out that silylene is a weak Lewis base.

4.2.2. Silylene as a Lewis Acid. The acidic strength of silylene was probed with NH_3 because this molecule is a strong Lewis base and is sufficiently small as not to suffer from steric constraints. For the complexes $Si_9H_{14}NH_3$, $Si_{16}H_{22}NH_3$, and $Si_{58}H_{62}NH_3$ the calculations provided the structures and VDD atomic charges shown in Figure 4 (left) and gave a bond-formation energy ΔE of −0.65 eV for the smallest, −0.58 eV for the intermediate, and −0.63 eV for the larger cluster, as reported in Table 7. The corresponding ΔH^0 values (−0.40 eV for $Si_9H_{14}NH_3$ and −0.30 eV for $Si_{16}H_{22}NH_3$) show an exothermic process. However, frequency calculation on $Si_{16}H_{22}NH_3$ gives one negative value; thus the structure is not a true minimum.

That the silanic hydrogen donates part of its charge to the neighboring silylene silicon is understood by observing that in the Lewis adduct (with Lewis formula $Si^--N^+H_3$, resulting from the reaction of the pristine cluster with NH_3) the bond between silanic hydrogen and silylene silicon is destroyed (see left of Figure 4). The negative nitrogen donates part of its charge to the empty p orbital of Si, saturating it to the extent that hydrogen cannot be attracted strongly enough. Both the silylene Si and silanic hydrogen bear negative charges, indicating the lack of nonconventional hydrogen bond.

4.3. Silylene as a Brønsted Acid. The Lewis formula of the silylene center suggests that each bridging hydrogen atom has an acidic nature, so that the cluster is expected to behave as a Brønsted acid (see ref 33 for a general theory of Brønsted acidity). If the silylene silicon has two silicon dihydrides as nearest neighbors, the center is expected to manifest resonance.

The acidic strength of silylene complexes was determined calculating the energy $W(1/n)$ for the heterolytic dissociation of the considered clusters:

$$Si_9H_{14} \xrightarrow{W(1/2)} Si_9H_{13}^- + H^+$$

$$Si_{16}H_{22} \xrightarrow{W(1/3)} Si_{16}H_{21}^- + H^+$$

$$Si_{58}H_{62} \xrightarrow{W(1/9)} Si_{58}H_{61}^- + H^+$$

with $(1)/(n)$ denoting the loss of 1 H^+ in the vicinity of 1 silylene on a surface of $n - 1$ silicon dihydrides. The calculations showed that in all cases the loss of the proton results in the

formation of a σ bond between the original silylene and the residual silicon monohydride (see Figure 5).

Formally, the negatively charged cluster admits a Lewis formula where the original silylene has a formal charge of -1. Table 8 summarizes the results of the calculations in terms of the energy of heterolytic dissociation W and neutralization energy of the negative ion E_{neu}.

The first information that can be extracted from this table is the very strong Brønsted acidity of the silylene, especially if compared with that of strong acids like HBr ($W = 14.04$ eV, gas phase) or H_2SO_4 ($W = 13.30$ eV, gas phase).[33] Only superacids like $HSbF_6$ ($W = 11.46$ eV, gas phase[33]) are stronger acids.

The second point of interest starts from the following relationship, resulting from Born−Haber analysis of the heterolytic dissociation:

$$W^{M^-} = E_{ion}^{H} - E_{neu}^{M^-} + \Delta H_{diss}^{M-H} \quad (7)$$

where E_{ion}^{H} is the ionization energy of the hydrogen atom and ΔH_{diss}^{M-H} is the M−H bond dissociation enthalpy. The process of homolytic dissociation,

$$M-H \xrightarrow{\Delta H_{diss}^{M-H}} M + H$$

can actually be seen as formed by two steps: the homolytic dissociation of an Si−H bond (requiring a bond dissociation energy E_b^{Si-H}) followed by the relaxation of the structure with the formation of an Si−Si σ (releasing an energy E_b^{Si-Si}) bond similar to those characteristic of 2×1 reconstruction:

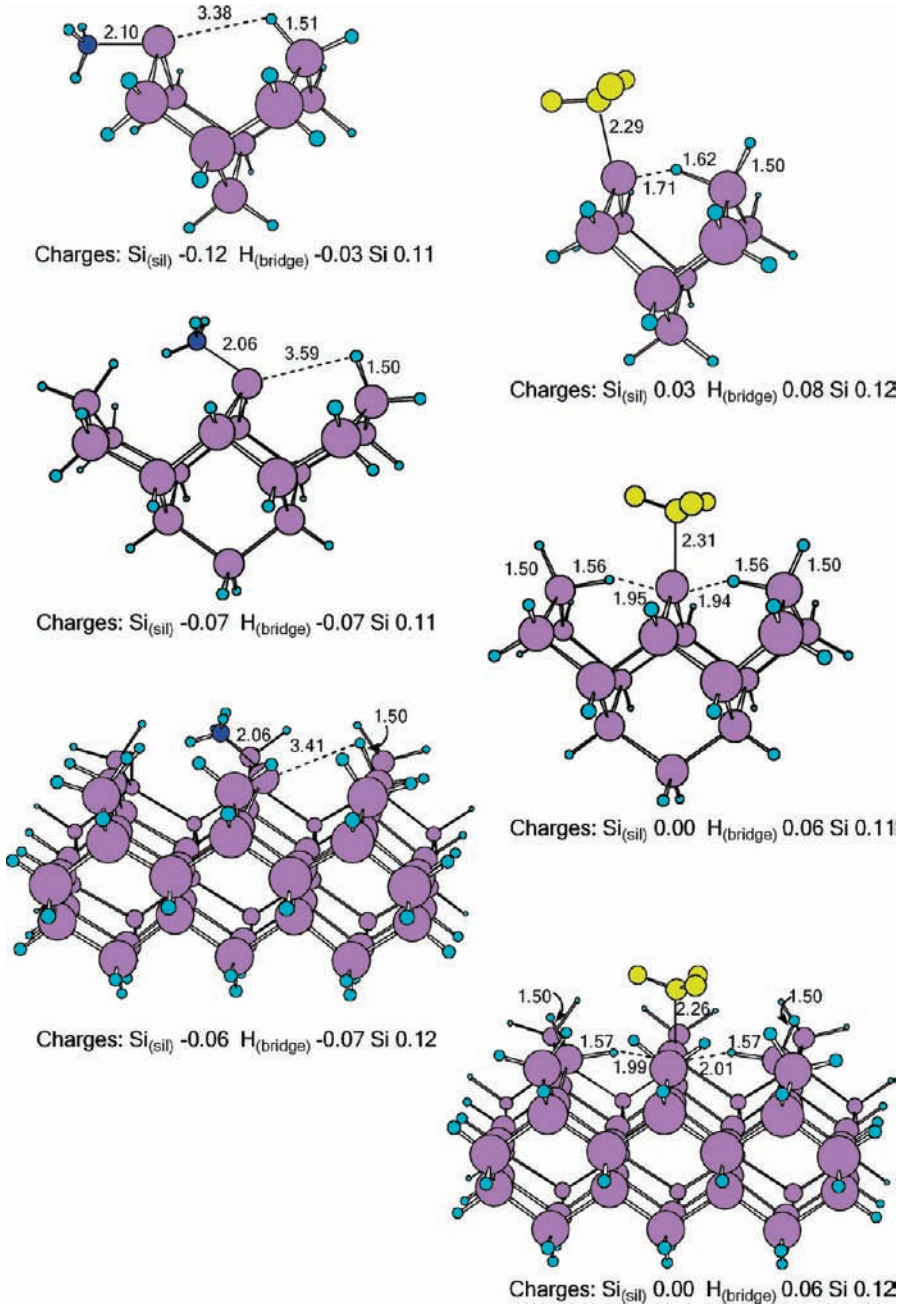

Figure 4. Formation of a Lewis adduct between a silylene cluster and NH_3 (left) or BF_3 (right), showing selected distances (in Å) and atomic charges for the three different size cluster models.

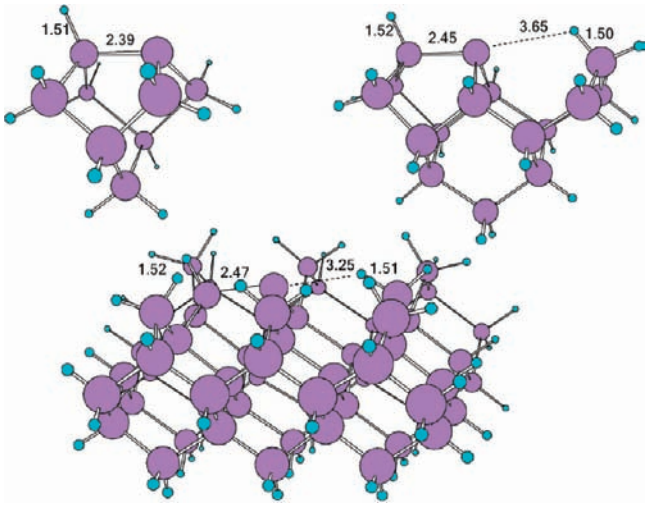

Figure 5. Structure and relevant distances (Å) in negatively charged silylene clusters of different sizes.

TABLE 7: Formation Energy ΔE (Gas Phase, 0 K, 0 atm), Enthalpy ΔH^0 (298 K, 1 atm), and Gibbs Free Energy ΔG^0 (298 K, 1 atm) of the Silylene Adducts with BF_3 (Top) and NH_3 (Bottom) as a Function of Cluster Size

	BF_3 adducts		
	Si_9H_{14}	$Si_{16}H_{22}$	$Si_{58}H_{62}$
ΔE (eV)	−0.13	−0.14	−0.15
ΔH^0 (eV)	−0.10	−0.14	
ΔG^0 (eV)	+0.37	+0.44	
	NH_3 adducts		
	Si_9H_{14}	$Si_{16}H_{22}$	$Si_{58}H_{62}$
ΔE (eV)	−0.65	−0.58	−0.63
ΔH^0 (eV)	−0.40	−0.30	
ΔG^0 (eV)	−0.05	+0.14	

TABLE 8: Energy for Heterolytic Dissociation W of Silylene Clusters and Neutralization E_{neu} of the Ion Resulting from the Heterolytic Dissociation

cluster	n	W (eV)	E_{neu} (eV)
Si_9H_{14}	2	12.98	2.75
$Si_{16}H_{22}$	3	12.81	2.98
$Si_{58}H_{62}$	9	12.41	3.44

$$\Delta H_{diss}^{M-H} \simeq E_b^{Si-H} - E_b^{Si-Si}$$

From $\Delta H_{diss}^{M-H} \simeq 2.2$ eV [from eq 7 and Table 8] and $E_b^{Si-H} \simeq 3.6$ eV, one gets $E_b^{Si-Si} \simeq 1.4$ eV, consistently with widespread view of the weakness of such a strained σ bond.

5. Stability in Atmospheric Moisture

It was already mentioned that the stability of silylene in the Si_9H_{14} and $Si_{16}H_{22}$ clusters was checked by verifying that all vibration modes have positive frequencies. For all clusters we calculated also the energy barrier separating the silylene defect from the monohydride dimer defect species along the reaction coordinate. The main result reported in our previous paper[10] was that the silylene species is expected to be observable at room temperature only for E^* higher than 0.7 eV, which is expected for d_{Si-H} larger than 2.16 Å.

At this stage we have no idea whether or not d_{Si-H} attains such a value by increasing the cluster size; the possibility of observing bare silylene at room temperature is essentially related to this occurrence.

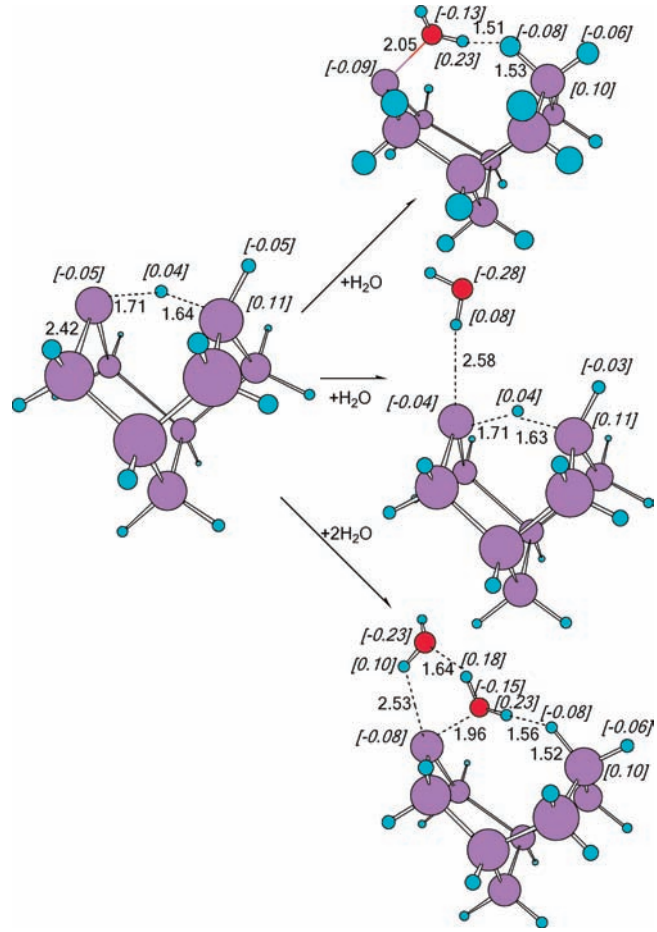

Figure 6. Complexes, with relevant atomic charges and selected distances (in Å), formed by reaction of one water with the acidic function of silylene (top) or with its basic function (middle), or by two water molecules (bottom) for the smallest cluster.

As discussed in the previous section, however, the silylene center may be stabilized via reaction with Lewis acids or bases. Among them water and hydroxyl anion are particularly interesting because they are certainly present when the surface is prepared via HF_{aq} etching and when the silylene prepared in dry conditions (as in ref 9) is exposed to atmospheric moisture.

Consistently with the zwitterionic nature of silylene, water is expected to react not only with the acidic function of silylene forming a Lewis adduct but also with its basic function with the formation of an ordinary hydrogen bond. Calculations showed that not only does water react with the acidic function of silylene silicon to form a center with Lewis formula $\rangle Si^- - O^+H_2$ but it also reacts with the basic function to form a hydrogen-bonded complex $\rangle Si^- \cdots HOH$. We calculated the complexes formed by reaction of one water molecule with the acidic function of silylene and with its basic function, and those formed by reaction of two water molecules with both acidic and basic function of silylene for all the three different size cluster models. The resulting complexes are depicted in Figures 6, 7, and 8 with selected geometrical parameters and relevant partial atomic charges. Binding energies are collected in Table 9.

The binding energies of one water molecule interacting with the basic function of silylene do not show dependence from the cluster size and are low: −0.11 eV for all clusters, the calculated ΔH^0 being −0.06 eV for both Si_9H_{14} and $Si_{16}H_{22}$ cluster models. The bonding energies of one water molecule interacting with the acidic function of silylene are −0.15 eV

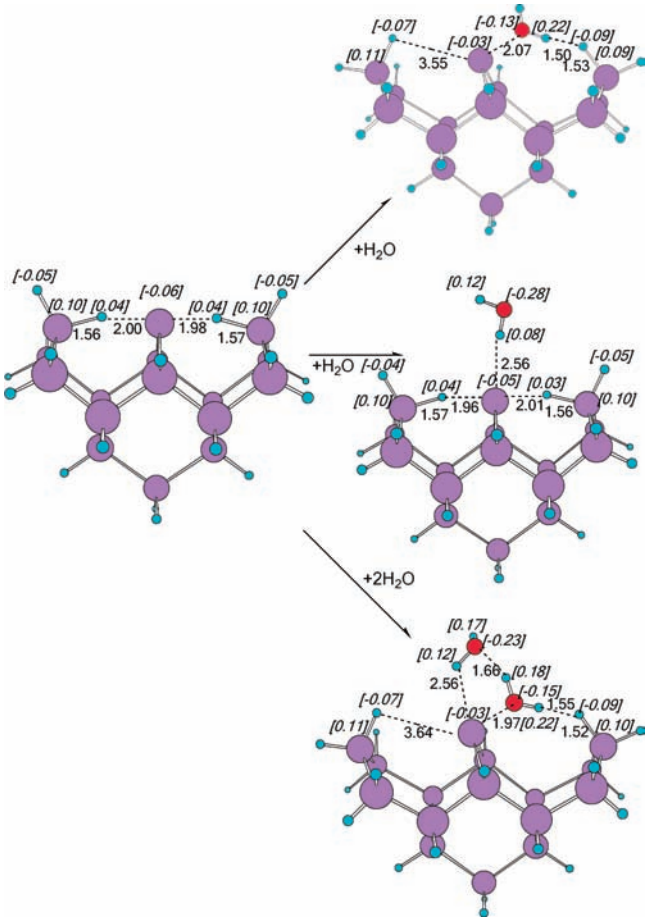

Figure 7. Complexes, with relevant atomic charges and selected distances (in Å), formed by reaction of one water with the acidic function of silylene (top) or with its basic function (middle), or by two water molecules (bottom) for the intermediate cluster.

for Si_9H_{14}, −0.11 eV for $Si_{16}H_{22}$, and −0.12 eV for $Si_{58}H_{62}$ cluster. In terms of ΔH^0 we calculate +0.03 eV and +0.13 eV for the Si_9H_{14} and $Si_{16}H_{22}$ cluster models, respectively.

Remarkably enough, the adsorption of two water molecules (respectively involving the acidic or basic functions) does stabilize the cluster. For the Si_9H_{14}, $Si_{16}H_{22}$, and $Si_{58}H_{62}$ clusters, indeed, the binding energies are −0.70, −0.63, and −0.67 eV, respectively, for the pair of H_2O molecules. The calculated ΔH^0 are −0.36 and −0.27 eV for the Si_9H_{14} and $Si_{16}H_{22}$ clusters, respectively, indicating an electronic stabilization. The water molecules are mutually bonded by a hydrogen bond, but the energy involved in that (of about 0.2 eV[34] (Table 3-1)) is insufficient to account for the reinforcement of the binding energy; the extra energy (of about 0.35 eV) is essentially due to the fact that a silylene bridge between the Lewis base $:OH_2$ and the acidic hydrogen H−OH amplifies the interaction energy. An additional inductive effect due to hydrogen bond between the two water molecules has also to be considered to contribute to stability.

To allow for the energetics of water reaction with silylene, one must take into account its evaporation enthalpy of ≃0.45 eV. If we include this value in the data shown in Table 9, we can observe that the reaction of silylene with liquid water would be in all cases an exothermic process, but strikingly, the corresponding ΔG^0 values would be still positive. We conclude that in experimental conditions liquid water does not interact with silylene.

Of course, none of the considered adducts, though being true minima, is the configuration of absolute minimum energy—the most stable configuration, indeed, implies the termination of silylene silicon with hydrogen and hydroxyl groups.

However, in our earlier work[10] we calculated the energy barrier to be overcome to allow the cleavage of the water to form hydrogen and hydroxyl terminations for the smallest cluster and the evaluated lifetime for that reaction was larger than 2×10^2 s. This estimate suggests that the reaction involving the cleavage of water does not forbid the observation of silylene at room temperature.

Another pathway eventually leading to the stabilization of the silylene involves the interaction with OH^- or with H_2O in a reaction where silylene behaves like boric acid; i.e., it accepts OH^- from water:

$$Si_9H_{14} + H_2O \xrightarrow{W(1/2)} [Si_9H_{14}(OH)]^- + H^+ \quad (8)$$

$$Si_{16}H_{22} + H_2O \xrightarrow{W(1/3)} [Si_{16}H_{22}(OH)]^- + H^+ \quad (9)$$

$$Si_{58}H_{62} + H_2O \xrightarrow{W(1/9)} [Si_{58}H_{62}(OH)]^- + H^+ \quad (10)$$

Table 10 shows that, whichever is the cluster size considered in reactions 8−10, the energy required for releasing the proton is higher for the dehydrated silylene than for the silylene−water complex. In a way, though the formation of the water adduct removes the Lewis acidity of the center, this process results in a stronger Brønsted acid.

Reactions can alternatively be written as follows

$$Si_9H_{14} + 2H_2O \xrightarrow{\Delta E(1/2)} [Si_9H_{14}(OH)]^- + H_3O^+ \quad (11)$$

$$Si_{16}H_{22} + 2H_2O \xrightarrow{\Delta E(1/3)} [Si_{16}H_{22}(OH)]^- + H_3O^+ \quad (12)$$

$$Si_{58}H_{62} + 2H_2O \xrightarrow{\Delta E(1/9)} [Si_{58}H_{62}(OH)]^- + H_3O^+ \quad (13)$$

Taking into account that the solvation energy of gas phase H_3O^+ is around −3.0 eV at room temperature, Table 10 guarantees that the silylene center is stable in water with respect to the formation of the [silylene−OH]$^-$ anion.

However, the high binding energy of the hydroxyl anion to silylene, shown in Table 9, is so high (−4.62 eV for Si_9H_{14}, −4.85 eV for $Si_{16}H_{22}$, and −5.39 eV for $Si_{58}H_{62}$, with a Gibbs free energy of −4.15 eV for Si_9H_{14} and −4.29 eV for $Si_{16}H_{22}$) to suggest this process as the etching mechanism of silicon in basic solution at high pH. For all the three different size cluster models, the [silylene−OH]$^-$ complexes with selected geometrical parameters and relevant atomic charges are depicted in Figure 9. The images show that the strong interaction with hydroxyl anion involves not only the acidic function of silylene but also its basic function, simultaneously, in a situation reminiscent of that of the adsorption of two water molecules.

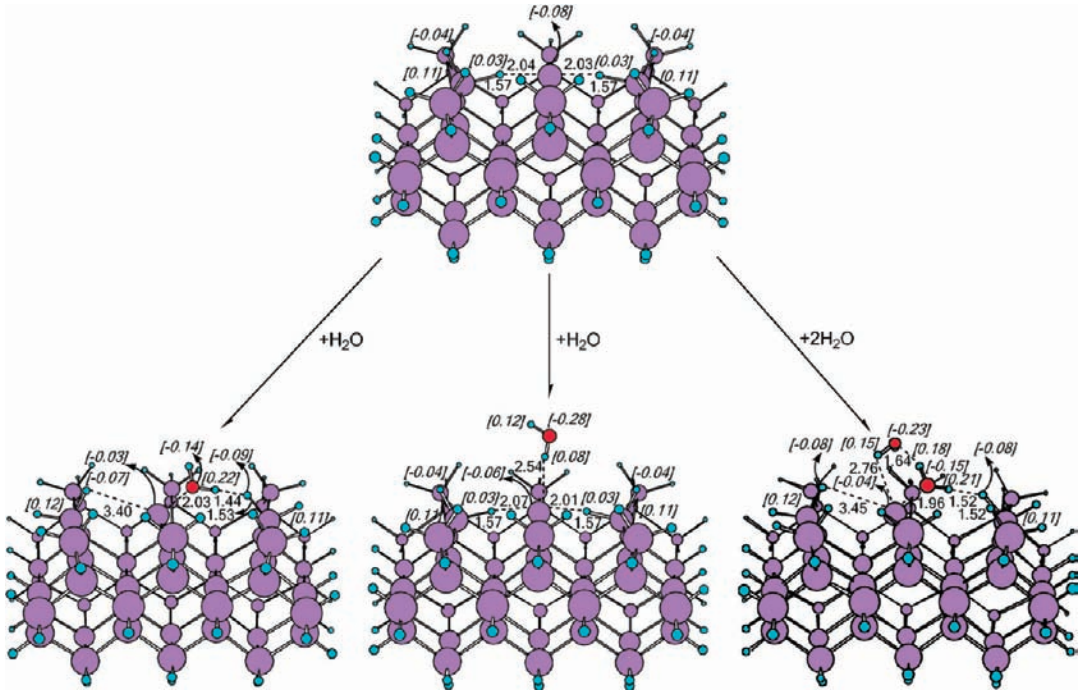

Figure 8. Complexes, with relevant atomic charges and selected distances (in Å), formed by reaction of water with the acidic function of silylene (left) or with its basic function (middle), or by two water molecules (right) for the largest cluster.

TABLE 9: Formation Energy ΔE (Gas Phase, 0 K, 0 atm) (in eV), Enthalpy ΔH^0 (298 K, 1 atm) (in eV), and Gibbs Free Energy ΔG^0 (298 K, 1 atm) (in eV) of the Silylene Adducts with One Water Molecule Interacting with the Acidic Function of Silylene, with Its Basic Function, of the Silylene Adducts with Two Water Molecules, and with Hydroxyl Anion[a]

cluster	$\Delta E(H_2O_{acidic})$	$\Delta E(H_2O_{basic})$	$\Delta E(2H_2O)$	$\Delta E(OH^-)$
Si_9H_{14}	−0.15	−0.11	−0.70	−4.62
$Si_{16}H_{22}$	−0.11	−0.11	−0.63	−4.85
$Si_{58}H_{62}$	−0.12	−0.11	−0.67	−5.39
	$\Delta H^0(H_2O_{acidic})$	$\Delta H^0(H_2O_{basic})$	$\Delta H^0(2H_2O)$	$\Delta H^0(OH^-)$
Si_9H_{14}	+0.03	−0.06	−0.36	−4.45
$Si_{16}H_{22}$	+0.13	−0.06	−0.27	−4.69
	$\Delta G^0(H_2O_{acidic})$	$\Delta G^0(H_2O_{basic})$	$\Delta G^0(2H_2O)$	$\Delta G^0(OH^-)$
Si_9H_{14}	+0.43	+0.37	+0.46	−4.15
$Si_{16}H_{22}$	+0.48	+0.37	+0.59	−4.29

[a] To allow for the energetics of water reaction with silylene, one must take into account its evaporation enthalpy of ≃0.45 eV.

Moreover, it is interesting to note how the negative charge on silylene Si rapidly decreases as the cluster size increases, thus pointing out the presence of a silylene band embedded in the conduction band of silicon.

A very strong acidity of silylene has been found. These facts suggest that the states of silylene datively bonded to adsorbed hydroxyl anion, a base species certainly present in atmospheric moisture, are sufficiently stable to be observable at room temperature even in a vacuum.

6. Does Silylene (and in Affirmative Case, in Which Configuration) Account for Feature $Si^{-\prime}$?

To verify which configuration (if any) of the silylene center may be held responsible for the XPS feature $Si^{-\prime}$, we describe the dependence of the chemical shift $\Delta\xi_i$ of the ith atom on its net charge Q_i through eq 18 of Appendix A.

To verify whether or not a certain silylene species may reasonably be assumed to account for feature $Si^{-\prime}$, it would be sufficient to calculate its net charge and truncated Madelung potential for a small cluster (consistent with those of Figure 2) and verify if the corresponding chemical shift, calculated with eq 19 of Appendix A, reproduces the experimental one, of −0.27 eV.

We have thus calculated by means of eq 19 the chemical shifts for the following species:

- silylene hydrogen-bonded to nearby silanic hydrogen, referred to as sil···H,
- silylene acid bonded to one water molecule, referred to as sil···OH_2,
- silylene base bonded to one water molecule, referred to as sil···HOH, and

TABLE 10: Energies W, ΔE (Gas Phase, 0 K, 0 atm), Enthalpy ΔH^0 (298 K, 1 atm), and Gibbs Free Energy ΔG^0 (298 K, 1 atm) for Heterolytic Dissociation of Water Induced by Silylene Clusters

cluster	n	W (eV)	ΔE (eV)	ΔH^0 (eV)	ΔG^0 (eV)
Si_9H_{14}	2	12.85	5.48	5.66	5.99
$Si_{16}H_{22}$	3	12.62	5.25	5.41	5.85
$Si_{58}H_{62}$	9	12.08	4.71		

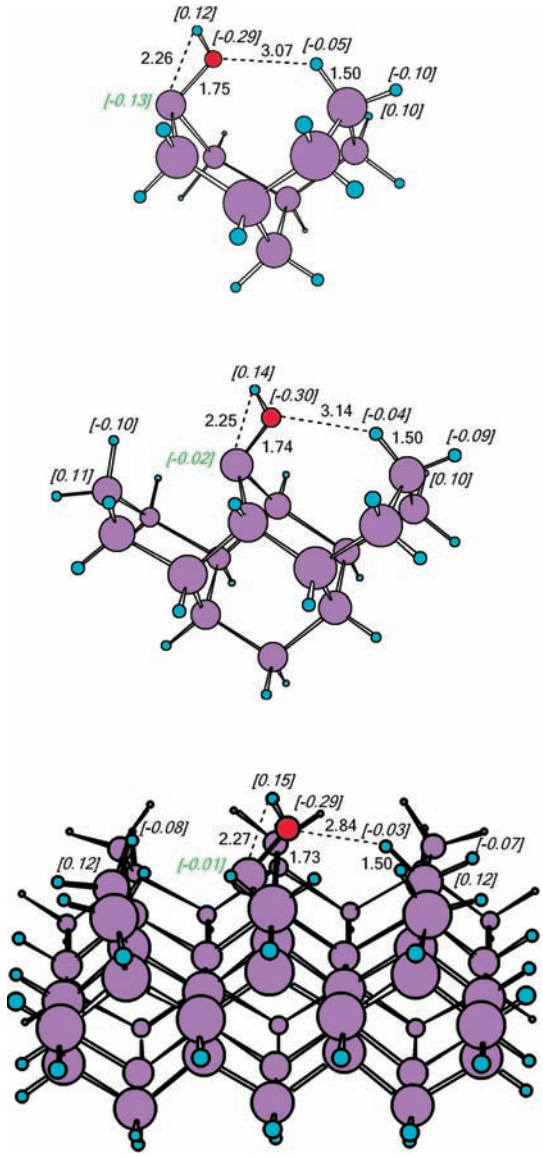

Figure 9. Complexes, with relevant atomic charges and selected distances (in Å), formed by reaction of hydroxyl anion with the acidic function of silylene for the three different size cluster models.

- Zwitterionic silylene bonded to two water molecules, referred to as sil···$(H_2O)_2$.

All the considered clusters are shown, with relevant distances and Voronoi charges, in Figure 10.

Charges, truncated Madelung potentials, and calculated chemical shifts of the considered silylene species are listed in Table 11.

It should be noted that we verified that the quantities of interest in these calculations (namely, Voronoi charges and interatomic distances) vary weakly with cluster size (see Appendix A). For sil···OH^- the chemical shift depends heavily on cluster size; however, whichever cluster is considered, one has $\Delta\xi < -1.36$ eV, which exclude this species from being a plausible candidate.

The table clearly shows that all species where silylene is coordinated with one or more water molecules cannot account for feature $Si^{-\prime}$; rather, the calculated chemical shift of bare silylene sil···H is consistent with the one of $Si^{-\prime}$.

At last we observe that the smallest model cluster shown in Figure 10 is already adequate to assess the assignment of the $Si^{-\prime}$ feature to the sil···H species.

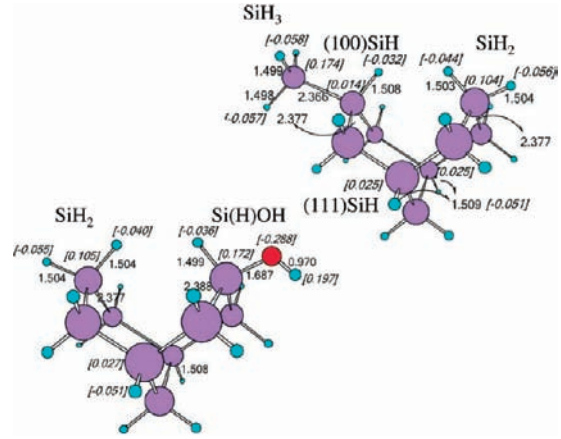

Figure 10. Clusters used for the calculation of the charge distribution on the considered hydrogen-terminated silicon atoms.

TABLE 11: Voronoi Charge, Truncated Madelung Potential, and Calculated Chemical Shift of the Considered Silylene Species

species	Q	$U^{(1)}$ (eV)	$\Delta\xi$ (eV)
sil···H	−0.05	+0.56	−0.10
sil···HOH	−0.04	+1.49	+0.89
sil···OH_2	−0.09	−1.78	−3.05
sil···$(H_2O)_2$	−0.08	−1.00	−2.12
$Si^{-\prime}$			−0.27

7. Conclusions

Density functional calculations for both periodic slabs and different size clusters have demonstrated that the loss of one H_2 molecule from an otherwise perfect unreconstructed, dihydrogen terminated, (100) surface of silicon may result in the formation of a metastable silylene center. A comparison between the two approaches to model the (100) Si surface shows that the considered clusters are useful models for an extensive chemical feature analysis of the isolated silylene defect. In the absence of other species the silylene center interacts strongly with neighboring silanic hydrogen, imparting to them an acidic character. Whether or not the species reverts at room temperature to the mohydride dimer defect depends critically on the silylene−hydrogen distance. The silylene center is stabilized, even at room temperature, via the adsorption of species like hydroxyl anions present in the HF_{aq}-etching solution. On the other hand, in experimental conditions adsorption of liquid water molecules on silylene is not a spontaneous process. Of the various silyene configurations, the bare silylene only might account for the feature with negative chemical shift observed by XPS at the hydrogen-terminated (100) silicon surface.

Appendix A. Assigning XPS Features to Chemical Species

With the remarkable exception of hydrogen, XPS is sensitive to all elements and the survey spectra provide sufficiently accurate, although mediated by the inelastic electronic collisions, knowledge of the elemental composition of the sampled region. Measurements at different takeoff angles or excitation energies combined with a knowledge of the electron mean free path can thus be used for the determination of the in-depth distributions of the various atoms.[35,36] Atoms of the same element may, however, have different bonding configurations, thus manifesting different chemical shifts $\Delta\xi$ with respect to the atom in an elemental state. In the absence of more detailed information, the configurations are tentatively given assuming the *naive assignation* (NA): for any atom $\Delta\xi$ increases in proportion to

its net charge Q determined in the hypothesis that its charge is the algebraic sum of the charges transferred along each bond due to the local electronegativity difference. The weight of the various configurations are then assigned consistently with the overall stoichiometry as results from XPS elemental analysis.

Elementary electrostatic considerations, however, show that $\Delta\xi$ depends not only on Q but also on the charge distribution on all neighboring atoms through the Madelung potential U, so that the attribution of XPS lines to bonding configurations guided by charge alone may be invalidated.

Lines could unambiguously be assigned to configurations if both Q and U were known. However, U can be determined only if the surface structure is known, that would render impossible any guess on surface structure unless *U is controlled (although not completely determined) by the nearest neighbors of the considered atoms.*

The theory is developed as follows. Assume that one is able to assign to each atom its net charge Q; for the ith atom the dependence of $\Delta\xi_i$ on Q_i is given by the following equation[37,38]

$$\Delta\xi_i = \epsilon_i Q_i + U_i + \mathcal{C} \tag{14}$$

where ϵ_i is the core−frontier coupling constant (an atomic property), $\mathcal{C}$ is the polarization energy (due to the polarization of the substrate when a core hole is formed after the photoemission, a substrate property), and U_i is the Madelung potential:

$$U_i = 2E_0 a_0 \sum_{j\neq i} \frac{Q_j}{|\mathbf{r}_j - \mathbf{r}_i|} \tag{15}$$

where $2E_0$ and a_0 are the atomic units of energy and length ($E_0 = 13.6$ eV and $a_0 = 0.53$ Å), $\mathbf{r}_j$ is the position of the jth atom, and the sum is extended to all atoms but the ith. The value of ϵ_i can be estimated from elementary electrostatics: assuming for simplicity that the charge basin is spherical with radius R_i and core electrons are distributed very close to the nucleus, one has

$$\varepsilon_i = \begin{cases} 3E_0 a_0/R_i \text{ for Q uniformly distributed inside sphere} \\ 2E_0 a_0/R_i \text{ for Q uniformly distributed on the sphere surface} \end{cases} \tag{16}$$

Since electrostatic repulsion spreads as much as possible the net charge, the first case in eq 16 is expected to be an overestimate of ϵ_i; on another side, ϵ_i cannot be lower than predicted by the second case of eq 16: $2E_0 a_0/R_i < \epsilon_i < 2E_0 a_0/R_i$. However, to be an atomic property R_i cannot be larger than the atomic radius a_i, so that

$$2E_0 a_0/a_i < \epsilon_i < 3E_0 a_0/a_i \tag{17}$$

Since for silicon $a_{Si} = 1.17$ Å, eq 17 suggests that ϵ_{Si} is in interval 12.3−18.5 eV. In the analysis of ref 38, ϵ_{Si} was found of the order of 17 eV (within ±40%). When confusion is impossible, ϵ (without any index) will be the contracted form of ϵ_{Si}.

Using eq 14 requires a knowledge of all Q_j and of the structure of the solid generating U_i. The solution to the inverse problem would be facilitated if the chemical shift of the ith atom were controlled by its first N nearest neighbors [referred to as $I^{(N)}(i)$] and the Madelung potential generated by the other atoms did not depend on the state of the considered atom. Rewrite now eq 14 in the following form:

$$\Delta\xi_i = \epsilon_i Q_i + U_i^{(N)} + V_i^{(\bar{N})} \tag{18}$$

where $U_i^{(N)}$ is the Madelung potential generated by the first, second, ..., Nth nearest neighbors to atom i,

$$U_i^{(N)} = 2E_0 a_0 \sum_{j\neq i, j\in I^{(N)}(i)} \frac{Q_j}{|\mathbf{r}_j - \mathbf{r}_i|}$$

and $V_i^{(\bar{N})}$ is the sum of the polarization energy with the Madelung potential generated by the remaining atoms (the upper index "$(\bar{N})$" denotes that it includes all atoms but the first, second, ..., Nth nearest neighbors to i, $\{j | j \notin I^{(N)}(i)\}$,

$$V_i^{(\bar{N})} = 2E_0 a_0 \sum_{j\neq i, j\notin I^{(N)}(i)} \frac{Q_j}{|\mathbf{r}_j - \mathbf{r}_i|} + \mathcal{C}$$

The interest in eq 18 resides in the *hope* that $V_i^{(\bar{N})}$ is nearly independent of i, $\forall i(V_i^{(\bar{N})} \simeq V^{(\bar{N})})$, so that eq 18 becomes

$$\Delta\xi_i \simeq \epsilon_i Q_i + U_i^{(N)} + V^{(\bar{N})} \tag{19}$$

Equation 19 is trivially rigorous for $N \rightarrow +\infty$ and is expected to provide an adequate description of the chemical shift taking for N the order of neighbors over which the surface may be viewed as homogeneous.

In ref 10 we assumed without discussion the NA ($N = 0$). In the following we make a little step further considering the case $N = 1$.

Assigning net charges to atoms, on the basis of Mulliken population analysis, is now believed to be useless due to heavy basis-set dependence; in recent years, however, another criterion, based on Voronoi tasselation, has been proved to provide more realistic descriptions of charge distribution on atoms in molecules.

To assign a net charge to atoms at hydrogen-terminated (100) Si surface, we used the clusters of fused cyclohexasilanes[21,39] shown in Figure 10. Both clusters may be used for modeling the SiH_2 center, the top cluster is used to model the SiH_3 center, and the bottom cluster is used to model the SiOH center (to the best of our knowledge, never considered in the literature). How modeling the SiH center is less trivial: the top cluster shows indeed not only a silicon monohydride resulting from the substitution of a silyl group for hydrogen at an otherwise perfect 1×1 (100) surface site [referred to as (100) SiH] but also two silicon monohydrides with symmetry and orientation characteristic of silicon monohydrides at the (111) surface [referred to as (111) SiH].

The use of small clusters is crucial for consistency with a description, like that of eq 19, where the Madelung potential is truncated at the first neighbors. Of course, this description has a meaning only if the resulting charge (albeit approximate) does not vary excessively when the cluster size is increased. We verified that the quantities of interest in this work (namely, Voronoi charges and interatomic distance) vary weakly with cluster size. For instance, Voronoi charges on SiH_2 and SiH_3 are +0.104 and +0.174, respectively, in $Si_{10}H_{18}$, or +0.103 and

TABLE 12: Charge, Madelung Potential and Expected Chemical Shifts (Apart from the Additive Term $V^{(\bar{1})}$ and for ϵ at the Extremes of Its Expected Validity Interval) of the Considered Surface Centers

			$\epsilon Q + U^{(1)}$ (eV)	
center	Q	$U^{(1)}$ (eV)	$\epsilon = 12.3$ eV	$\epsilon = 18.5$ eV
(100) SiH	0.014	+0.753	+0.952	+1.012
(111) SiH	0.025	−0.487	−0.180	−0.025
SiH_2	0.104	−0.958	+0.321	+0.966
Si(H)OH	0.172	−2.804	−0.688	+0.378
SiH_3	0.174	−1.577	+0.563	+1.642

TABLE 13: Considered Assignation Schemes[a]

	Line				
	$Si^{-\prime}$	$Si^{\prime}$	$Si^{2\prime}$	$Si^{3\prime}$	Si^{1}
	Assignation				
NA		SiH	SiH_2	SiH_3	Si(H)OH
CIA_4		SiH	SiH_2	Si(H)OH	SiH_3
CIA_3		SiH	Si(H)OH	SiH_2	SiH_3
CIA_2		Si(H)OH	SiH	SiH_2	SiH_3
CIA_1	Si(H)OH	SiH	SiH_2	SiH_3	

[a] In all cases line Si^1 has a contribution due to $Si(OSi^n)$.

+0.188 in $Si_{17}H_{26}$; for a still larger cluster, with 58 silicon atoms, SiH_2 was calculated to have $Q = 0.114$.

The net charges Q on the surface atoms and their nearest neighbor distances are shown in the stick-and-ball pictures in Figure 10. This figure allows $U^{(1)}$ to be calculated for all configurations; ignoring the net charges on silicon atoms mimicking "bulk" atoms, we list charges and truncated Madelung potentials on the silicon configurations of interest for this work in the second and third columns of Table 12.

Ignoring for a moment the center (100) SiH and denoting since now on (111) SiH simply with SiH, we observe that, irrespective of the assumed value of ϵ in the considered interval, the putative chemical shift $\Delta\xi$ ($=\epsilon Q + U^{(1)}$, except for the additive term $V^{(\bar{1})}$) increases in the order $\Delta\xi[\mathrm{SiH}] < \Delta\xi[\mathrm{SiH_2}] < \Delta\xi[\mathrm{SiH_3}]$. Rather, the value of ϵ affects only the position of Si(H)OH in the sequence: the order shifts from $\Delta\xi[\mathrm{Si(H)OH}] < \Delta\xi[\mathrm{SiH}] < \Delta\xi[\mathrm{SiH_2}] < \Delta\xi[\mathrm{SiH_3}]$ for $\epsilon = 12.3$ eV [the lowest value in the confidence interval resulting from estimate (16)], to $\Delta\xi[\mathrm{SiH}] < \Delta\xi[\mathrm{Si(H)OH}] < \Delta\xi[\mathrm{SiH_2}] < \Delta\xi[\mathrm{SiH_3}]$ for $\epsilon = 18.5$ eV [the largest value in the confidence interval resulting from estimate (16)].

Thus together with the naive assignment NA, resulting from Pauling charge on silicon from the electronegativity distribution on nearest neighbors, we consider in Table 13 four counterintuitive assignments (CIA_1, CIA_2, CIA_3, and CIA_4) characterized by the different positions of Si(H)OH in the silicon−hydride alignment. For them one has

- $\epsilon = 16.11$ eV and $V^{(\bar{1})} = +0.01$ eV, with $r = 0.819$ for NA;
- $\epsilon = 16.19$ eV and $V^{(\bar{1})} = +0.01$ eV, with $r = 0.938$ for CIA_4;
- $\epsilon = 15.32$ eV and $V^{(\bar{1})} = +0.11$ eV, with $r = 0.967$ for CIA_3;
- $\epsilon = 13.84$ eV and $V^{(\bar{1})} = +0.29$ eV, with $r = 0.968$ for CIA_2; and
- $\epsilon = 11.54$ eV and $V^{(\bar{1})} = +0.24$ eV, with $r = 0.956$ for CIA_1.

On going from NA to CIA_4 the quality of the statistical description is improved in the following order:

$$\mathrm{NA} \ll \mathrm{CIA_4} < \mathrm{CIA_1} < \mathrm{CIA_3} \simeq \mathrm{CIA_2}$$

The statistical descriptions of CIA_2 and CIA_3 are nearly the same, and they provide the optimal description. However, CIA_2 must be discarded because the assignment of Si′ to SiH is guaranteed by the syncrotron-radiation XPS data of Karlsson and co-workers, who for the (111) SiH surface measured $\Delta\xi = +0.19$ eV.[40] Taking into account that the HF_{aq} etching of the native oxide of (100) Si results in (111) facets and the their hydrogen termination, we may confidently assign Si′ to (111) SiH. We are thus forced to accept CIA_3 (the one in Table 2) that, however, leaves $Si^{-\prime}$ unassigned.

Acknowledgment. This work was supported by MIUR (FIRB 2003: Molecular compounds and hybrid nanostructured materials with resonant and non resonant optical properties for photonic devices) and by INSTM-CNR (PROMO project).

References and Notes

(1) Neergaard Waltenburg, H.; Yates, J. T. *Chem. Rev.* **1995**, *95*, 1589.
(2) Jo, S. K.; Kang, J. H.; Yan, X.-M.; White, J. M.; Eckerdt, J. G.; Keto, J. W.; Lee, J. *Phys. Rev. Lett.* **2000**, *85*, 2144.
(3) Aoyama, T.; Goto, K.; Yamazaki, T.; Ito, T. *J. Vac. Sci. Technol. A* **1996**, *14*, 2909.
(4) Cerofolini, G. F.; Galati, C.; Lorenti, S.; Renna, L.; Viscuso, O.; Bongiorno, C.; Raineri, V.; Spinella, C.; Condorelli, G. G.; Fragala, I. L.; Terrasi, A. *Appl. Phys. A: Mater. Sci. Process.* **2003**, *77*, 403.
(5) Niwano, M.; Kageyama, J.; Kinashi, K.; Takashi, I.; Miyamoto, N. *J. Appl. Phys.* **1994**, *76*, 2157.
(6) Cerofolini, G. F.; Giussani, A.; Carone Fabiani, F.; Modelli, A.; Mascolo, D.; Ruggiero, D.; Narducci, D.; Romano, E. *Surf. Interface Anal.* **2007**, *39*, 836.
(7) Cerofolini, G. F.; Romano, E.; Giorgi, G.; Belanzoni, P. *Chem. Phys. Lett.*, submitted for publication.
(8) Cerofolini, G. F.; Galati, C.; Renna, L. *Surf. Interface Anal.* **2003**, *35*, 968.
(9) Cerofolini, G. F.; Galati, C.; Reina, S.; Renna, L.; Spinella, N.; Jones, D.; Palermo, V. *Phys. Rev. B* **2005**, *72*, 125431.
(10) Cerofolini, G. F.; Giorgi, G.; Sgamellotti, A.; Belanzoni, P. *J. Chem. Phys.* **2009**, *130*, 184702.
(11) Cerofolini, G. F.; Meda, L. *Appl. Surf. Sci.* **1995**, *89*, 351.
(12) Fonseca Guerra, C.; Handgraaf, J. W.; Baerends, E. J.; Bickelhaupt, F. M. *J. Comput. Chem.* **2004**, *25*, 189.
(13) Ordejón, P.; Artacho, E.; Soler, J. M. *Phys. Rev. B* **1996**, *53*, R10441.
(14) Soler, J. M.; Artacho, E.; Gale, J. D.; García, A.; Junquera, J.; Ordejón, P.; Sànchez-Portal, D. *J. Phys.: Condens. Matter* **2002**, *14*, 2745.
(15) http://www.icmab.es/siesta
(16) Perdew, J. P.; Burke, K.; Ernzerhof, M. *Phys. Rev. Lett.* **1996**, *77*, 3865.
(17) Trouiller, N.; Martins, J. L. *Phys. Rev. B* **1991**, *43*, 1993.
(18) Rurali, R. *Phys. Rev. B* **2005**, *71*, 205405.
(19) Markussen, T.; Rurali, R.; Jauho, A.-P.; Brandbyge, M. *Phys. Rev. Lett.* **2007**, *99*, 076803.
(20) Monkhorst, H. J.; Pack, J. D. *Phys. Rev. B* **1976**, *13*, 5188.
(21) Konecny, R.; Hoffman, R. *J. Am. Chem. Soc.* **1999**, *121*, 7918.
(22) Becke, A. D. *Phys. Rev. A* **1988**, *38*, 3098.
(23) Perdew, J. P. *Phys. Rev. B* **1986**, *33*, 8822.
(24) Perdew, J. P. *Phys. Rev. B* **1986**, *34*, 7406.
(25) ADF2007.01, SCM, Theoretical Chemistry, Vrije Universiteit Amsterdam, The Netherlands, 2007; http://www.scm.com.
(26) Baerends, E. J.; Ellis, D. E.; Ros, P. *Chem. Phys.* **1973**, *2*, 42.
(27) te Velde, G.; Bickelhaupt, F. M.; van Gisbergen, S. J. A.; Fonseca Guerra, C.; Baerends, E. J.; Snijders, J. G.; Ziegler, T. *J. Comput. Chem.* **2001**, *22*, 931.
(28) Fonseca Guerra, C.; Snijders, J. G.; te Velde, G.; Baerends, E. J. *Theor. Chem. Acc.* **1998**, *99*, 391.
(29) te Velde, G.; Baerends, E. J. *J. Comput. Phys.* **1992**, *99*, 84.
(30) Alkorta, I.; Rozas, I.; Elguero, J. *Chem. Soc. Rev.* **1998**, *27*, 163.
(31) Raghavachari, K.; Chandrasekhar, J.; Frisch, M. J. *J. Am. Chem. Soc.* **1982**, *104*, 3779.
(32) Raghavachari, K.; Chandrasekhar, J.; Gordon, M. S.; Dykema, K. J. *J. Am. Chem. Soc.* **1984**, *106*, 5853.
(33) Cerofolini, G. F.; Marrone, A.; Re, N. *J. Mol. Structure: THEOCHEM* **2007**, *810*, 121.
(34) Cotton, F. A.; Wilkinson, G. *Advanced Inorganic Chemistry*, 5th ed.: Wiley: New York, 1988.

(35) Seah, M. P.; Briggs, D. *Practical Surface Analysis: Auger and X-Ray Photoelectron Spectroscopy*, 2nd ed.; Wiley: Chichester, 1992.

(36) Briggs, D.; Grant, J. T. *Surface Analysis by Auger and X-ray Photoelectron Spectroscopy*; IMPublications: Chichester, U.K., 2003.

(37) Nefedov, V. I.; Yarzhemsky, V. G.; Chuvaev, A. V.; Trishkina, E. M. *J. Electron Spectrosc. Relat. Phenom.* **1988**, *46*, 381.

(38) Cerofolini, G. F.; Meda, L.; Re, N. *Appl. Phys. A: Mater. Sci. Process.* **2001**, *72*, 603.

(39) Hess, J. S.; Doren, D. J. *J. Phys. Chem. B* **2002**, *106*, 8206.

(40) Karlsson, C. J.; Owman, F.; Landemark, E.; Chao, Y.-C.; Uhrberg, R. I. G. *Phys. Rev. Lett.* **1994**, *72*, 4145.

JP903433E